Quantum-Assisted Combinatorial Optimization for Reconfigurable Intelligent Surfaces in Smart Electromagnetic Environments

Qi Jian Lim, Student Member, IEEE, Charles Ross, Student Member, IEEE, Amitava Ghosh, Fellow, IEEE, Frederick Vook, Senior Member, IEEE, Gabriele Gradoni, Member, IEEE, and Zhen Peng, Senior Member, IEEE

Abstract—We have recently seen a surge in interest in leveraging reconfigurable intelligent surfaces in smart radio environments. One critical question is how to efficiently optimize the phase configuration that results in the desired reflective wavefront. In this paper, we proposed a physics-based optimization approach inspired by the statistical mechanics of correlated spins and adiabatic quantum computing. The new concept is based on the isomorphism of electromagnetic scattered power and the Ising Hamiltonian. As a result, the problem of optimizing phase configuration is transformed into the problem of finding the ground state of the target Ising Hamiltonian. We successfully demonstrate the feasibility of combinatorial optimization for weighted beamforming and diffusive scattering applications using this framework.

Index Terms—Electromagnetic metamaterials, diffusive scattering, Ising model, optimization, reconfigurable intelligent surface, weighted beamforming, wireless communication, 6G.

I. INTRODUCTION

RECONFIGURABLE intelligent surfaces (RISs) are software-controlled large engineered surfaces with many low-cost passive reflecting elements, where the desired reflective wavefront may be achieved by tuning the local reflection phase and/or amplitude of individual elements [1]–[8]. Recently, we have seen a growing interest in using RISs to dynamically manipulate the propagation environment [9]–[18]. Going beyond 5G and entering 6G, it is envisioned that large-scale, distributed RIS devices will be deployed at the surface of interacting objects, e.g. walls, windows, furniture, in the propagation channel [19]–[21]. The overall goal is to transform the radio environment into a smart and reconfigurable space

The work is supported by U.S. National Science Foundation (NSF) CAREER Award, #1750839, NSF ECCS-EPSRC award, #2152617, Nokia University Donations program, and U.S. Office of Naval Research (ONR) Award #N00014-20-1-2835. The work of G.G. was supported in part by the European Union's Horizon 2020 Industrial leadership project RISE-6G, No. 101017011, and in part by the Royal Society Industry Fellowship INF\R2\192066. (Corresponding author: Zhen Peng)

- Q.J. Lim, C. Ross, and Z. Peng are with the Center for Computational Electromagnetics, Department of Electrical and Computer Engineering, University of Illinois at Urbana-Champaign, Urbana, IL 61801 USA (e-mail: qjlim2@illinois.edu; cr26@illinois.edu; zvpeng@illinois.edu).
- G. Gradoni is with the School of Mathematical Sciences, and the George Green Institute for Electromagnetics Research, Department of Electrical and Electronics Engineering, University of Nottingham, Nottingham NG7 2RD, U.K., and he is also an adjunct associate professor at the Department of Electrical and Computer Engineering, University of Illinois at Urbana-Champaign, Urbana, IL 61801 USA (e-mail: gabriele.gradoni@nottingham.ac.uk)
- A. Ghosh and F. Vook are with the NOKIA Standards at Nokia Bell Labs, Naperville, IL, 60563 (e-mail: amitava.ghosh@nokia-bell-labs.com, fred.vook@nokia-bell-labs.com)

that provides enhanced coverage with high energy efficiency and supports ultra-fast and seamless connectivity.

To fully realize the potential of RIS-enabled smart electromagnetic (EM) environment, one needs to rapidly find the optimal states of RIS with prescribed objective functions. While there are mathematical tools like generalized Snell's law for anomalous reflection [4], there are no semi-analytical solutions for specific EM functionalities, e.g., multi-beamforming, energy focusing, diffusive scattering, and wireless functionalities, such as spatial diversity, data throughput, and physical-layer security. Therefore, various RIS optimization methods have been proposed in the literature, including genetic algorithms [22]-[24], impedance-based synthesis [25], electromagnetic inversion [26], machine learning [27]-[32], as well as dynamical optimization [33]-[36]. Despite these advances, it is still considered a challenging computational optimization task due to the enormous number of RIS configurations, the complexity of EM scattering environments, and the processing time constraints for wireless systems and networks.

Recently, significant advancements in quantum computing (QC) algorithms and hardware provide a novel paradigm for solving difficult computational problems. Regarding EM applications, the quantum Fourier Transform was used for antenna array synthesis [37]. A quantum method of moment approach based on the Harrow/Hassidim/Lloyd (HHL) algorithm is developed for the characterization of interconnects [38], [39]. Variational quantum algorithms with the finite difference method are presented for the calculation of waveguide modes [40]. In terms of wireless networks, quantum computing and optimization are used for multi-user MIMO detection and processing [41], [42] and optimal resource allocation for 6G wireless network [43].

The proposed work stands on the fusion of statistical mechanics models with QC algorithms to overcome the high computational optimization complexity in the RIS-aided smart radio environment. The philosophy is to recast the RIS-aided wireless and/or EM problem into a physical formulation that can be tackled efficiently with emerging QC hardware [44]. As an example, the Ising model is widely used in statistical mechanics to describe the spin state of quantum particle arrays. In [45], we expand on this analogy and develop an Ising model for the RISs with beamforming/nullforming applications. By designing the Ising Hamiltonian to mimic EM scattered power, the optimal RIS configuration is encoded in the ground state solution of the Ising spin system, which can be effectively

found by heuristic quantum optimization algorithms.

In this paper, we advance this area of research in three directions. First, we evaluate and benchmark the performance of quantum optimization algorithms against classical heuristic algorithms. Second, we go beyond the basic beamforming applications and demonstrate the feasibility of the proposed methodology for weighted beamshaping and diffusive scattering applications. The emphasis is placed on the development of Ising Hamiltonian models in practical scenarios of wireless communication and radar engineering. Third, we discuss the use of hybrid classical-quantum algorithms for large-scale Ising optimization problems. The research outcomes are expected to be important in the emerging fields of large-scale smart EM environments and new wireless infrastructures, including high-capacity networks with reduced emission levels, smart skins for EM wave signal processing, and directed energy countermeasures to high-power EM coupling.

II. BACKGROUND

A. Introduction to Ising Model

The Ising spin lattice model is originally introduced as a mathematical model for understanding ferromagnetism in statistical mechanics [46]. The magnetic moments of atomic spins are represented by discrete variables, +1 for the spin up and -1 for the spin down. In the Ising model, the energy objective function (also called Hamiltonian) is expressed as a quadratic function of spin vector $\{s_1, s_2, \dots, s_M\}$:

$$H = \sum_{m=1}^{M} \sum_{n=m+1}^{M} s_m s_n J_{mn} + \sum_{m=1}^{M} h_m s_m$$
 (1)

where the spin variables $s_m \in \{+1, -1\}$ express the two orientations for each moment. The entries J_{mn} , also called couplers, characterize the interaction energy of moments m and n, and the entries h_m , also called bias, refer to local magnetic fields that act individually on the s_m . In principle, a variety of combinatorial optimization problems can be expressed as the energy minimization of an appropriate Ising spin model by properly choosing the J_{mn} and h_m [47].

B. Ising Model for RIS Beamforming

We consider the basic problem statement of a RIS-assisted wireless network as illustrated in Fig. 1, including a user's equipment (UE), a base station (BS), and a passive RIS array. The BS controls the operation of the RIS through an out-of-band control channel [48] to the RIS controller. The RIS unit cells are individually connected to the RIS controller that implements tunability of local reflection phases to incoming waves. Namely, one can tune the reflection phase of each RIS element from a finite set of phase states, e.g., 1-bit (binary) RIS can be tuned with a reflection phase of 0° or 180°, and a 2-bit RIS element exhibits four reflection phase states. As such, we can view the RIS optimization as an integer programming model, which searches for an optimal solution over all the combinatorial states of RIS elements.

To briefly demonstrate the method, we consider an Melement linear RIS array with the application of desired signal

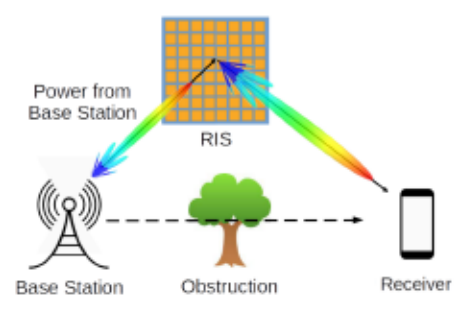


Fig. 1: A RIS-assisted wireless network for creating a virtual line-of-sight between the BS and the UE.

maximization towards the elevation angle of θ^s and azimuthal angle of ϕ^s . The scattered EM field can be written as: $\mathbf{E} = \sum_{m=1}^{M} \mathbf{G}_m(\theta,\phi)s_m$, where the RIS basis state s_m represents the element phase modulation, e.g. ± 1 corresponding to the $0/\pi$ phase response, and the $\mathbf{G}_m(\theta,\phi)$ is the element-wise scattering vector that can be calculated by the physical optics (PO) approximation or the full-wave numerical method. We can then express the EM scattered power as a quadratic model:

$$P(\theta, \phi) = \mathbf{E}^{\dagger} \cdot \mathbf{E} = \sum_{m=1}^{M} \sum_{n=1}^{M} \mathbf{G}_{m}^{\dagger}(\theta, \phi) \mathbf{G}_{n}(\theta, \phi) s_{m} s_{n}$$
 (2)

From this, we can construct an energy maximization Hamiltonian with an order 2 polynomial. By using symmetry in the scattering vector, the effective Hamiltonian can be constructed as an Ising spin-glass model:

$$H(\theta^{s}, \phi^{s}) = -P(\theta^{s}, \phi^{s}) = \sum_{m=1}^{M} \sum_{n=m+1}^{M} s_{m} s_{n} J_{mn}(\theta^{s}, \phi^{s})$$
(3)

in which the desired scattering direction is denoted by θ^s and ϕ^s . The computation of spin-spin interaction strength, J_{mn} , is detailed in [45] and skipped here for brevity.

The solution to the RIS beamforming problem can be found by solving an argmin optimization problem:

$$\hat{s}_1, \cdots, \hat{s}_M = \operatorname*{argmin}_{s_1, \cdots, s_M} H(\theta^s, \phi^s) \tag{4}$$

which is equivalent to finding the ground state of the Ising Hamiltonian.

C. Heuristic Quantum Optimization Algorithm

Generally speaking, finding the ground state of an Ising model is an NP-hard (non-deterministic polynomial-time hard) problem due to the exponentially large solution space, i.e. $O(2^M)$ for 1-bit RIS and $O(4^M)$ for 2-bit RIS. Classical optimization algorithms [49]–[51] do not scale well with a large number of RIS elements. To find the ground-state solution effectively, one appealing way forward is to leverage recent advances in the adiabatic QC hardware, so-called quantum annealer (QA) [52], which received considerable interest lately due to the number of available qubits and programmability [41], [53]–[56].

The QA is a type of analog quantum computing processor (QPU) that specializes in solving NP-hard combinatorial optimization problems. The principles of operation are derived from the adiabatic theorem [57], which states that a quantum system in its ground state will remain in the ground state, provided the Hamiltonian governing the dynamics changes sufficiently slowly. Applying this to the Ising model, one may initialize the quantum system in the ground state of a Hamiltonian that is known and easy to prepare, and slowly change it to a complex Ising Hamiltonian that encodes the optimization problem. The final state of the system, which is the ground state of the Ising Hamiltonian, represents the optimal solution to the problem.

The particular physical QA hardware considered in this work is the D-Wave Advantage system [58], which has 5,000 functional quantum bits (qubits) represented by circulating currents in superconducting loops. The Ising model is compiled into the D-Wave QA device through a process of embedding and de-embedding. The corresponding quantum Hamiltonian with Ising spins in a transverse field is given by:

$$\mathcal{H}(t) = -\mathcal{A}(t) \left(\sum_{m=1}^{M} \hat{\sigma}_{m}^{\mathbf{x}} \right) + \mathcal{B}(t) \left(\sum_{m=1}^{M} \sum_{n=m+1}^{M} \hat{\sigma}_{m}^{\mathbf{z}} \hat{\sigma}_{n}^{\mathbf{z}} \bar{J}_{mn} \right) \tag{5}$$

where $\hat{\sigma}_m^{\mathrm{x,z}}$ are the Pauli spin matrices. The $\hat{\sigma}_m^z$ represent the spin projections along either the $+\mathrm{z}$ or $-\mathrm{z}$ direction. The $\mathcal{A}(t)$ stands for the transverse Hamiltonian due to an applied transverse field in the x-direction. The quantum annealing process starts at time t=0 with $\mathcal{A}(0)\gg\mathcal{B}(0)$. The system is then evolved adiabatically by decreasing $\mathcal{A}(t)$ and increasing $\mathcal{B}(t)$ until the annealing time t_f is reached. If the increase in \mathcal{B} is slow enough, the adiabatic theorem ensures that the final state of the system is the ground state of the target Hamiltonian. Namely, the qubits have dephased to classical systems, and the $\hat{\sigma}_m^z$ can be replaced by classical spin variables, \hat{s}_m , which indicates the optimal configuration of RIS.

It is noted that due to the undesired noise on the quantum processors in an open environment, it is difficult to fulfill the precise adiabaticity condition in practice. Because of the non-adiabatic effects, there is no theoretical guarantee that QA will find the ground state (i.e. an optimal solution) for each annealing cycle. But the global optimality may be reached with high probability [45]. As a result, the QA is considered a heuristic quantum optimization algorithm.

III. WEIGHTED MULTIPLE BEAMFORMING

A. Motivation for Weighted Beamforming

Recently, non-orthogonal multiple access (NOMA) is introduced for the design of radio access techniques in fifthgeneration (5G) and beyond wireless networks [59], [60]. The central idea behind NOMA is that multiple users can share the same frequency and time resources, resulting in increased spectral efficiency. NOMA schemes are broadly classified into two types: code-domain multiplexing and power-domain multiplexing. The code-domain multiplexing allows for multiple transmissions by assigning different codewords to different users. It's thus crucial to distribute the power necessary to balance the channel conditions in order to guarantee user fairness. In the power-domain NOMA, multiuser signal data streams are superimposed at the transmitter side, and successive interference cancellation is used to decode the signals at

the receiver side. Multiple access is achieved by allocating different power levels to different users' signal data, taking advantage of channel gain differences among users.

In this study, we aim to exploit the RIS's configurability to generate weighted multiple beamforming, such that either heterogeneous channel conditions desired by power-domain NOMA or homogeneous channel conditions required by codedomain NOMA can be achieved at will. An example of RIS-aided code-domain NOMA is shown in Fig. 2. There are multiple mobile receivers that simultaneously require a considerable amount of signal energy from the transmitting base station. To ensure user fairness, we want the RIS to redirect signals from a single base station to distribute appropriate signal power to receivers. In particular, the RIS may be configured to perform beamforming towards nearer receivers with lower signal power and beamforming towards farther receivers with higher signal power. Consequently, all mobile receivers can meet the required minimum signal-to-noise ratio.

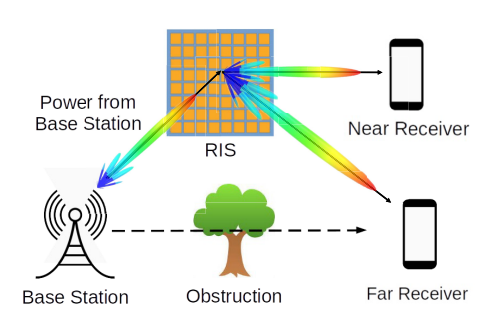


Fig. 2: RIS-aided code-domain NOMA wireless network.

B. Construction of Ising Hamiltonian

Given the problem statement in Fig. 2, an extension of (3) can be formulated as an Ising Hamiltonian for weighted beamforming of a 2-D rectangular M by N RIS panel. The scattered EM field can be written as $\mathbf{E}(\theta,\phi) = \sum_{m=1}^{M} \sum_{n=1}^{N} \mathbf{G}_{mn}(\theta,\phi) s_{mn}$, where s_{mn} and $\mathbf{G}_{mn}(\theta,\phi)$ are the RIS spin variable and element-wise scattering response, respectively, for RIS element at the m^{th} row and n^{th} column of the RIS panel. In addition, assuming the desired scattering directions towards two receivers are (θ_1^s,ϕ_1^s) , and (θ_2^s,ϕ_2^s) , we can define the weighted scattering field differential as:

$$\bar{\mathbf{E}}(\theta_1^s, \phi_1^s, \theta_2^s, \phi_2^s, W) = \mathbf{E}(\theta_1^s, \phi_1^s) - W\mathbf{E}(\theta_2^s, \phi_2^s)$$
 (6)

in which a weighting factor W is introduced to account for the desired difference between the scattered field intensities from the RIS towards two angular directions. The scattered power differential is defined as:

$$P_d = \bar{\mathbf{E}}^{\dagger}(\theta_1^s, \phi_1^s, \theta_2^s, \phi_2^s, W) \cdot \bar{\mathbf{E}}(\theta_1^s, \phi_1^s, \theta_2^s, \phi_2^s, W)$$
 (7)

4

Next, we can construct the Ising Hamiltonian for weighted beamforming by the following equation:

$$H = -P(\theta_1^s, \phi_1^s) - P(\theta_2^s, \phi_2^s) + \Lambda P_d(\theta_1^s, \phi_1^s, \theta_2^s, \phi_2^s, W)$$
(8)

$$= (1 - \Lambda) \sum_{u=1}^{M} \sum_{v=1}^{N} \sum_{m=1}^{M} \sum_{n=1}^{N} \bar{J}_{mnuv}(\theta_1^s, \phi_1^s) s_{uv} s_{mn}$$

$$+ (1 - W^2 \Lambda) \sum_{u=1}^{M} \sum_{v=1}^{N} \sum_{m=1}^{M} \sum_{n=1}^{N} \bar{J}_{mnuv}(\theta_2^s, \phi_2^s) s_{uv} s_{mn}$$

$$+ 2W \Lambda \Re \left[\sum_{v=1}^{M} \sum_{v=1}^{N} \sum_{m=1}^{M} \sum_{n=1}^{N} \bar{J}_{mnuv}^d(\theta_1^s, \phi_1^s, \theta_2^s, \phi_2^s) s_{uv} s_{mn} \right]$$
(9)

where the spin-spin interaction strengths are obtained by:

$$\bar{J}_{mnuv}(\theta_1^s, \phi_1^s) = -\mathbf{G}_{uv}^{\dagger}(\theta_1^s, \phi_1^s)\mathbf{G}_{mn}(\theta_1^s, \phi_1^s) \quad (10)$$

$$\bar{J}_{mnuv}(\theta_2^s, \phi_2^s) = -\mathbf{G}_{uv}^{\dagger}(\theta_2^s, \phi_2^s)\mathbf{G}_{mn}(\theta_2^s, \phi_2^s) \quad (11)$$

$$\bar{J}_{mnuv}^d(\theta_1^s, \phi_1^s, \theta_2^s, \phi_2^s) = -\mathbf{G}_{uv}^{\dagger}(\theta_1^s, \phi_1^s)\mathbf{G}_{mn}(\theta_2^s, \phi_2^s) \quad (12)$$

In (8), the beam power maximization in both desired directions is carried out by the first two terms. The scattering power difference between two beams is enforced by the third term. The penalty factor Λ strikes a balance between the beam power maximization and the beam weighting in terms of the energy objective functions.

C. Extension of the Ising Model to 2-bit RIS

The above procedure can be extended to RISs with higher-order phase modulation. Taking the quadriphase RIS as an example, the element reflection coefficient has four quantized phase states with a $\pi/2$ phase increment, therefore it is often referred to as 2-bit reflecting element. The element-wise response can be represented by two Ising spin variables, $s_{mn}^{\rm Re} \in \pm 1$ and $s_{mn}^{\rm Im} \pm 1$ [45]. The scattered EM field can be written as:

$$\dot{\mathbf{E}} = \sum_{m=1}^{M} \sum_{n=1}^{N} \mathbf{G}_{mn}(\theta^s, \phi^s) \left(s_{mn}^{\text{Re}} + j s_{mn}^{\text{Im}} \right)$$
(13)

It is noted that the scattering field is defined as $\dot{\mathbf{E}}$ in order to minimize confusion with symbols used in the previous subsection. The dot symbol is used to indicate terms for 2-bit RIS applications. Compared to (2), the EM scattered power for the 2-bit RIS is expressed as:

$$\dot{P}(\theta,\phi) = \dot{\mathbf{E}}^{\dagger}(\theta,\phi) \cdot \dot{\mathbf{E}}(\theta,\phi)$$

$$= \sum_{u=1}^{M} \sum_{v=1}^{N} \sum_{m=1}^{M} \sum_{n=1}^{N} \left[\mathbf{G}_{uv}^{\dagger}(\theta,\phi) \mathbf{G}_{mn}(\theta,\phi) s_{uv}^{\mathrm{Re}} s_{mn}^{\mathrm{Re}} + j \mathbf{G}_{uv}^{\dagger}(\theta,\phi) \mathbf{G}_{mn}(\theta,\phi) s_{uv}^{\mathrm{Re}} s_{mn}^{\mathrm{Im}} - j \mathbf{G}_{uv}^{\dagger}(\theta,\phi) \mathbf{G}_{mn}(\theta,\phi) s_{uv}^{\mathrm{Im}} s_{mn}^{\mathrm{Re}} + \mathbf{G}_{uv}^{\dagger}(\theta,\phi) \mathbf{G}_{mn}(\theta,\phi) s_{uv}^{\mathrm{Im}} s_{mn}^{\mathrm{Im}} \right]$$

$$+ \mathbf{G}_{uv}^{\dagger}(\theta,\phi) \mathbf{G}_{mn}(\theta,\phi) s_{uv}^{\mathrm{Im}} s_{mn}^{\mathrm{Im}} \right]$$

$$(14)$$

The weighted scattered power differential is defined as:

$$\dot{P}_d = \dot{\bar{\mathbf{E}}}^{\dagger}(\theta_1^s, \phi_1^s, \theta_2^s, \phi_2^s, W) \cdot \dot{\bar{\mathbf{E}}}(\theta_1^s, \phi_1^s, \theta_2^s, \phi_2^s, W) \tag{15}$$

where $\bar{\mathbf{E}}$ is the weighted scattering field differential:

$$\dot{\mathbf{E}}(\theta_1^s, \phi_1^s, \theta_2^s, \phi_2^s, W) = \dot{\mathbf{E}}(\theta_1^s, \phi_1^s) - W\dot{\mathbf{E}}(\theta_2^s, \phi_2^s)$$
(16)

We can then construct the Ising Hamiltonian for the weighted beamforming application. Due to the involvement of multiple spin-spin interaction definitions in the formulation, we simplify the expression of the Hamiltonian as summations of two types of sub-hamiltonians, H_e and H_d , in which H_e is related to the energy hamiltonian that maximizes the power in the desired direction and H_d is the sub-hamiltonian responsible for enforcing the weighing constraints between the two beams.

$$H = -\dot{P}(\theta_1^s, \phi_1^s) - \dot{P}(\theta_2^s, \phi_2^s) + \Lambda \dot{P}_d(\theta_1^s, \phi_1^s, \theta_2^s, \phi_2^s, W)) = (1 - \Lambda)H_e(\theta_1^s, \phi_1^s) + (1 - W^2\Lambda)H_e(\theta_2^s, \phi_2^s) + 2W\Lambda\Re[H_d]$$
(17)

where $H_e(\theta^s,\phi^s)=-\dot{P}(\theta^s,\phi^s)$ and

$$H_{d} = \sum_{u=1}^{M} \sum_{v=1}^{N} \sum_{m=1}^{M} \sum_{n=1}^{N} \left[\bar{J}_{mnuv}^{RR,d}(\theta_{1}^{s}, \phi_{1}^{s}, \theta_{2}^{s}, \phi_{2}^{s}) s_{uv}^{\text{Re}} s_{mn}^{\text{Re}} + \bar{J}_{mnuv}^{RI,d}(\theta_{1}^{s}, \phi_{1}^{s}, \theta_{2}^{s}, \phi_{2}^{s}) s_{uv}^{\text{Re}} s_{mn}^{\text{Im}} + \bar{J}_{mnuv}^{IR,d}(\theta_{1}^{s}, \phi_{1}^{s}, \theta_{2}^{s}, \phi_{2}^{s}) s_{uv}^{\text{Im}} s_{mn}^{\text{Re}} + \bar{J}_{mnuv}^{II,d}(\theta_{1}^{s}, \phi_{1}^{s}, \theta_{2}^{s}, \phi_{2}^{s}) s_{uv}^{\text{Im}} s_{mn}^{\text{Im}} + \bar{J}_{mnuv}^{II,d}(\theta_{1}^{s}, \phi_{1}^{s}, \theta_{2}^{s}, \phi_{2}^{s}) s_{uv}^{\text{Im}} s_{mn}^{\text{Im}} \right]$$
(18)

$$\bar{J}_{mnuv}^{RR,d}(\theta_1^s, \phi_1^s, \theta_2^s, \phi_2^s) = \mathbf{G}_{uv}^{\dagger}(\theta_1^s, \phi_1^s) \mathbf{G}_{mn}(\theta_2^s, \phi_2^s) \quad (19)$$

$$\bar{J}_{mnuv}^{RI,d}(\theta_1^s, \phi_1^s, \theta_2^s, \phi_2^s) = j\mathbf{G}_{uv}^{\dagger}(\theta_1^s, \phi_1^s)\mathbf{G}_{mn}(\theta_2^s, \phi_2^s) \quad (20)$$

$$\bar{J}_{mnuv}^{IR,d}(\theta_1^s, \phi_1^s, \theta_2^s, \phi_2^s) = -j\mathbf{G}_{uv}^{\dagger}(\theta_1^s, \phi_1^s)\mathbf{G}_{mn}(\theta_2^s, \phi_2^s) \quad (21)$$

$$\bar{J}_{mnuv}^{II,d}(\theta_1^s, \phi_1^s, \theta_2^s, \phi_2^s) = \mathbf{G}_{uv}^{\dagger}(\theta_1^s, \phi_1^s) \mathbf{G}_{mn}(\theta_2^s, \phi_2^s) \quad (22)$$

IV. DIFFUSE SCATTERING

A. Electromagnetic Signature Reduction

Besides beamforming and focusing in communication networks, the RIS can be of great value to other commercial and defense applications. One such example is the use of RIS as an EM stealth solution for military scenarios. The demand for light-weight and low-profile materials for stealth technology in military applications is ubiquitous. Absorbing materials have traditionally been used to reduce the EM signature of platforms. However, the performance of these materials typically scales with thickness. When the material thickness is a hard constraint, diffusive RIS is an appropriate alternative. By redirecting energy in all directions, the reflected EM energy is dispersed and thus reducing the monostatic EM signature, as illustrated in Fig. 3.

In the literature, the scaling laws and bounds on diffusive metasurfaces are discussed in [61]. A sub-optimal generalized Golay-Rudin-Shapiro (GRS) code is utilized to generate the 1-bit coding pattern for the case of normal plane wave incidence. As shown in Fig. 3, oblique incident fields may also impinge on the diffusive RIS mounted on the platform. Thus, it is important to assess the diffusive performance in such cases. In this section, we present a RIS-Ising model for diffuse scattering, which incorporates the attributes of element-specific scattering factor and angular-dependent excitation, and also can be efficiently solved by the quantum annealing algorithm.

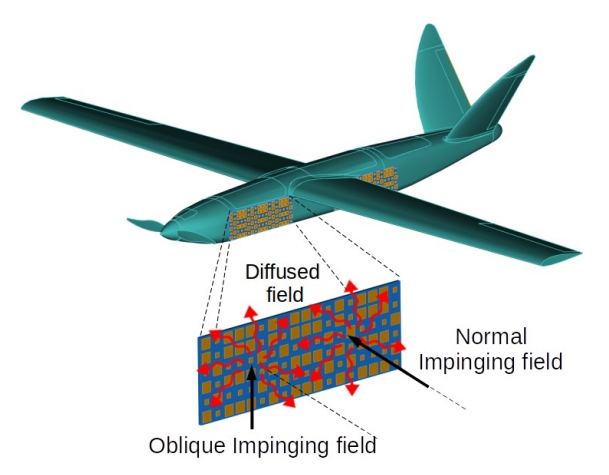


Fig. 3: Illustration of the diffusive RIS that reduces the EM signature of the platform.

B. Construction of Ising Hamiltonian

In the ideal case, a perfect diffusive scatterer would direct energy equally in all directions, resulting in a uniformly low diffused isotropic EM field. In other words, the scattered power would spread throughout the angular domain. Based on this observation, we aim to construct an Ising Hamiltonian that mimics the variance in the scattering densities.

The conventional way to compute the variance of a scattered power $P(\theta,\phi)$ in the angular domain follows the expected value of the squared deviation from the mean power: $\sigma^2 = \mathrm{E}\left[(P(\theta,\phi)-\bar{P})^2\right]$. However, this method may be impractical as the mean power \bar{P} is inaccessible. Alternatively, we first generate a finite sample of N angular observations, then construct a Hamiltonian associated with the population variance of the scattered power from the RIS:

$$H_{\text{var}} = \frac{1}{S^2} \sum_{i}^{S} \sum_{j>i}^{S} \left[P(\theta_i, \phi_i) - P(\theta_j, \phi_j) \right]^2$$
 (23)

whereby S represents the number of scattering angles used to compute the population variance of the scattered power. The obtained variance Hamiltonian is an energy function that describes the variance of the scattered power in the angular domain. The ground state solution (minimum value) of the Hamiltonian produces the desired scattering pattern with the lowest variance.

C. Reduction of Higher-order Interaction

From (23), we observe that the variance Hamiltonian requires the product of scattered powers $P(\theta,\phi)$, i.e. (2) for 1-bit RIS and (14) for 2-bit RIS. The result leads to the fourth order polynomial in the Ising model, also known as the four-body interaction among four Ising variables $s_m s_n s_i s_v$. The D-Wave QA hardware is not capable of solving these terms directly, as current annealers only allow polynomials with a maximum order of 2. Thus, we need to convert the fourth-order terms to second-order ones through a process of quadratization. Specifically, we have made use of a polynomial penalty approach, similar to methods introduced in [62], to

reduce higher-order terms to a sum of pairwise-interaction, two-body terms.

To briefly show the algorithm, we consider a four-body interaction term of $s_1s_2s_3s_4$, where s_i is the i^{th} Ising variable. The first step is to convert the four-body interaction term to a three-body interaction term by introducing 2 auxiliary spin variables and a weighted quadratic penalty function as follows:

$$s_1 s_2 s_3 s_4 = s_1 s_2 s_1^a + VP(s_3, s_4; s_1^a, s_2^a)$$
 (24)

where s_1^a and s_2^a are auxiliary variables. This step converts the four-body interaction term $s_1s_2s_3s_4$ to a three-body interaction term $s_1s_2s_1^a$ with a penalty weighting factor V and penalty function with pairwise interaction terms, s_is_j . The penalty function is expressed as $P(s_3,s_4;s_1^a,s_2^a)=4+s_3+s_4-s_1^a-2s_2^a+s_3s_4-s_3s_1^a-s_4s_1^a-2s_3s_2^a-2s_4s_2^a+2s_1^as_2^a$, which is used to enforce the constraint $s_1^a=s_3s_4$.

The next step in the process is to reduce the three-body interaction term $s_1s_2s_1^a$ to a sum of pairwise interaction terms. It involves introducing two new auxilliary variables s_3^a, s_4^a and another penalty function $P(s_2, s_1^a; s_3^a, s_4^a)$. The final expression of the fully quadratized four-body interaction term can be expressed as follows:

$$s_1 s_2 s_3 s_4 = s_1 s_3^a + VP(s_2, s_1^a; s_3^a, s_4^a) + VP(s_3, s_4; s_1^a, s_2^a)$$
 (25)

Figure 4 graphically illustrates this recursive quadratization process. In the graph, the blue nodes represent the original Ising variables related to the phase of each RIS element and the red nodes represent the auxiliary variables. The connected edges describe the pairwise interactions between these variables and the dashed box represents higher order interaction (four-body or three-body interactions) among the variables contained in the box. As shown in Fig. 4, four new auxiliary variables are added for each 4-body interaction term in the Hamiltonian. The result allows us to simulate the higher order Ising optimization problem using current quantum annealers.

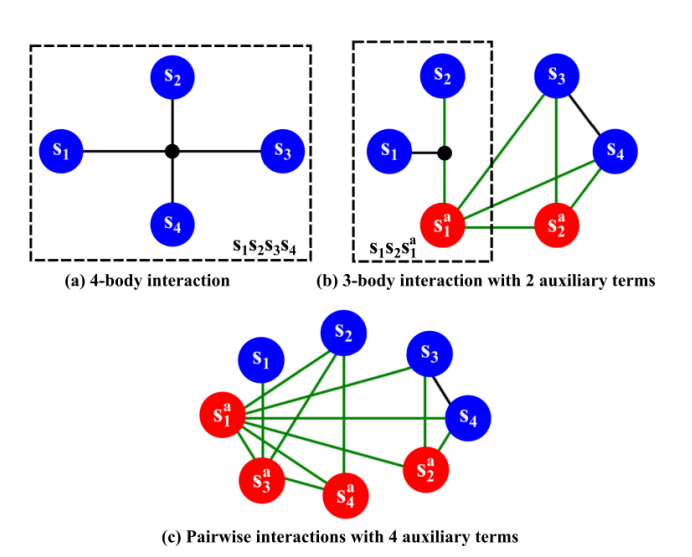


Fig. 4: Graph illustration of recursive quadratization process.

V. HYBRID CLASSICAL-QUANTUM ALGORITHMS

The D-Wave Advantage 4.1 QPU hardware consists of 5000 functional qubits that are coupled through a sparsely connected Pegasus topology [63]. Because our Ising model generates a fully connected graph (also known as a clique), a minor embedding process is required to convert the clique to the Pegasus lattice structure [64]. During the minor embedding, multiple physical qubits must be constrained to have the same value in order to represent a single Ising variable. As a result, the maximum RIS problem size we can simulate on the D-Wave QPU is at most 177 1-bit RIS elements or 88 2-bit RIS elements for beamforming operations. Assuming that we are interested in RIS panels with an equal number of RIS elements in both dimensions, this constraint translates to a maximum panel size of 13 by 13 1-bit RIS panel and 6 by 6 2-bit RIS panel. From this, we can see that current quantum computers lack the scale required for large RIS problems.

In the quantum computing community, several papers have proposed hybrid classical-quantum algorithms that make use of both classical and quantum computing hardware to optimize large-scale problems of interest [65]. For example, D-Wave has provided a reference hybrid classical-quantum solver named as Kerberos [66]. After decomposing the large-scale problem into subproblems, the solver concurrently performs Tabu search and simulated annealing algorithms on the classical computer and D-wave QA sampling on the quantum computer. The solver monitors all three optimization tracks and outputs the results from the fastest track.

In this paper, we explore a hybrid classical-quantum algorithm based on the large neighborhood search heuristic algorithm [67]–[69]. It is an iterative algorithm that searches for local solutions in a given neighborhood, which is defined as a subset cluster of variables in the original large problem. This process is repeated until the convergence criteria are met while exploring different neighborhoods of the problem. For the RIS beamforming application, we pick the sub-regions by sliding a fixed square frame across the RIS (Fig. 5). We then optimize RIS elements inside the frame to obtain a local solution for each sub-region. These local solutions will be merged to form the global solution.

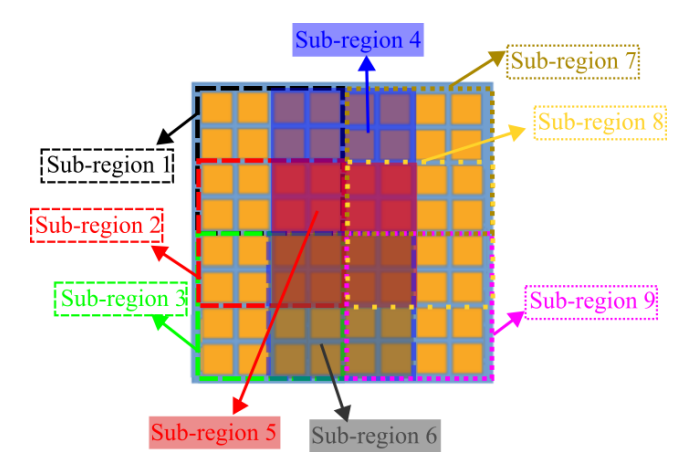


Fig. 5: Partition of the RIS panel into overlapping sub-regions for beamforming applications.

Special attention needs to be made to the diffusive scattering applications. Due to a large number of 4-body interaction terms, the straightforward sliding frame approach will cause significant information loss in the variance Hamiltonian. Thus, we propose two ingredients to improve the effectiveness of the hybrid classical-quantum algorithm for diffusive scattering cases. In the preparation stage, rather than forming regular subregions through regular spatial decomposition, we construct sub-regions by randomly selecting a subset of the entire problem. Figure 6 depicts the construction of two overlapping subregions. The first sub-region contains the first, second, fourth, and fifth RIS cells, whereas the second sub-region contains the first, third, fifth, and sixth RIS elements. Using this method, we can create randomized sub-region combinations while minimizing information loss in the variance Hamiltonian.

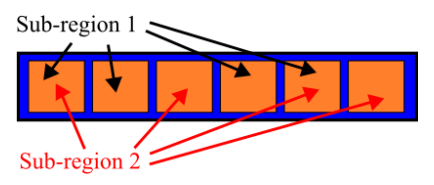


Fig. 6: Random partitioning of a 6-element 1D RIS array for diffusive scattering application.

Second, instead of a straightforward merge, we use a greedy-path merge at the end of every iteration. This is illustrated in Fig. 7. We apply quantum annealing to a particular RIS sub-region during each iteration. This allows us to obtain the initial RIS state prior to annealing as well as the updated RIS state after annealing. Next, we generate intermediate RIS states by following a greedy path between the RIS state before and after annealing. Among all of these RIS states, we select the RIS state with the lowest energy to update the initial RIS state for the next iteration. This procedure is repeated until all sub-regions have been optimized.

VI. NUMERICAL EXPERIMENTS

A. Performance Evaluation and Benchmarking

In this section, we will compare the performance of quantum annealing (QA) to that of classical algorithms, followed by a discussion of the use of hybrid quantum algorithms for large-scale Ising optimization problems.

1) Benchmarking with classical algorithms: The performance of QA is benchmarked against two classical algorithms, i.e. the simulated annealing (SA) [49] and the branch-and-bound algorithm [70]. To elaborate, the SA can be thought as a classical analog of quantum annealing. It involves implementing Metropolis-Hastings method with a temperature schedule. The particular SA solver used for this study is provided by DWAVE neal package [71]. The branch-and-bound solver used in this paper is from IBM's CPLEX Optimizer [72], which is a cutting-edge solver for Mixed Integer Program (MIP) problems. Both classical solver experiments were carried out on an Intel Core i7-1165G7 CPU. The QA is executed on the D-Wave Advantage 4.1 machine.

For this benchmarking experiment, we consider a TE polarized plane wave normally incident upon a one-dimensional

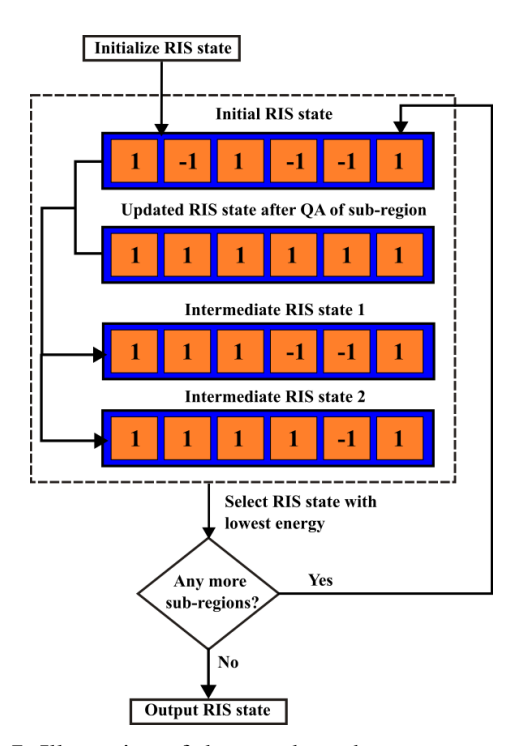


Fig. 7: Illustration of the greedy-path merge procedure.

RIS array with binary (1-bit) elements. The size of the RIS element is 1λ and the RIS elements are placed along the $\hat{\mathbf{y}}$ -axis. It is noted that the element size has been chosen to be comparable to the wavelength. In practice, the RIS panel design may start at the subwavelength unit cell level with the assumption of a local periodic arrangement. At deployment, each RIS element may consist of a number of subwavelength unit cells with the same switching states. A stable phase control can be approximated at the element level across discrete states. We aim to optimize the RIS phase profile, such that the scattered power is maximized at a desired direction ($\theta^s = 15^\circ, \phi^s = 90^\circ$). The obtained radar cross section (RCS) values for a variety of problem sizes are shown in Fig. 8, where the optimized solutions have very similar qualities.

The next task is to compare the time-to-solution (TTS) of the three methods. Given the probabilistic nature of QA and SA heuristics, the TTS is evaluated in two steps. For each of the problem instances, we first calculate the average success probability $\mathcal{P}_s(N)$ of finding the ground-state solution by performing 1000 runs (also called anneals). The minimum required number of runs to achieve a desired probability of success \mathcal{P}_d can then be calculated by:

$$R(N) = \frac{\ln(1 - \mathcal{P}_d)}{\ln(1 - \mathcal{P}_s(N))}$$
(26)

where N denotes the RIS array size and the desired probability \mathcal{P}_d is set to be 99.99% in our study. Finally, the TTS is calculated by multiplying R(N) with the time required for one run. Regarding the CPLEX Optimizer, the default settings are used in the study.

The TTS taken for the three methods are depicted in Fig. 9. We first observe that the CPLEX optimizer scales poorly

with RIS size. This insinuates that such a classical algorithm might not be suitable for RIS optimization problems. Next, we can see that SA is the fastest for small problems. As we increase the size of the RIS, the time required for SA increases noticeably. At around the array size of 128, QA takes over as the most efficient solver. The study suggests that QA has better scalable performance than the other solvers. This result encourages the investigation of quantum optimization algorithms for RIS-Ising models.

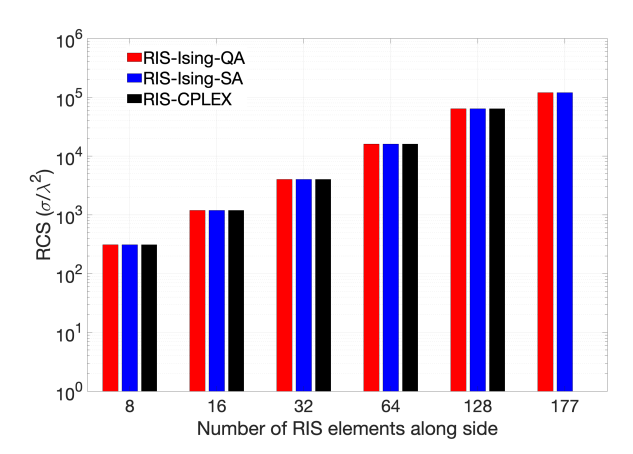


Fig. 8: Optimized RCS results from quantum annealing (RIS-Ising-QA), simulated annealing (RIS-Ising-SA) and IBM CPLEX optimizer (RIS-CPLEX).

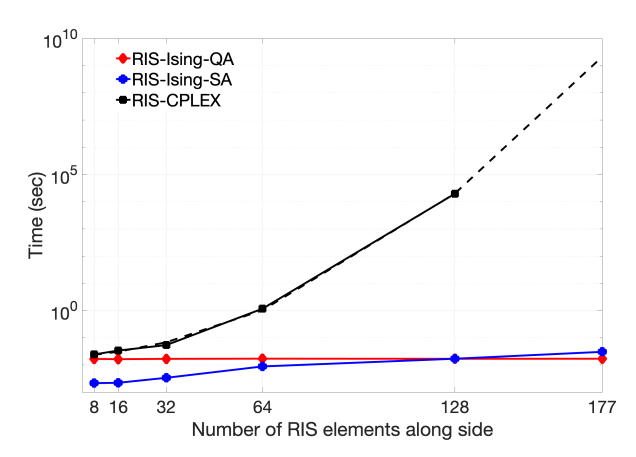


Fig. 9: Time-to-solution required by quantum annealing (RIS-QA), simulated annealing (RIS-SA), and IBM CPLEX optimizer (RIS-CPLEX).

2) Extension to large-scale Ising models: As discussed earlier, the problem size that can be solved by the QA is relatively small due to the mismatch between the fully connected graph generated by RIS Ising models and the sparse Pegasus graph used in D-Wave QPU hardware. A hybrid classical-quantum algorithm, denoted by the hybrid quantum annealing (HQA) method, is proposed in Section V to overcome the limitation.

We use the same benchmark problem as in the previous subsection to evaluate the performance of HQA and SA. The size of the RIS array ranges from 400 to 6400 elements. Figure 10 shows the obtained optimal RCS values. We see that the

HQA and SA achieve the same RCS values at the desired scattering angle. The TTS data for the two optimizers are given in Fig. 11. It is noted that the TTS for HQA includes both the QPU access time (for the QA optimization of sub-regions) and the CPU execution time (for merging the local solutions). We can see that the HQA generally takes less time than the SA. A 37.9 times runtime speedup is achieved for the problem size of 6400 RIS elements.

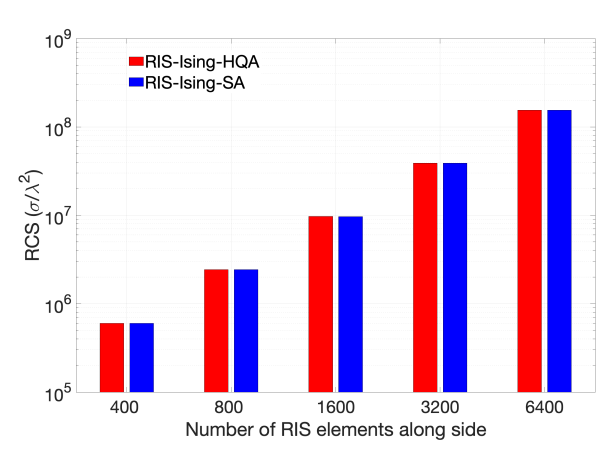


Fig. 10: Optimized RCS results from hybrid quantum annealing (RIS-Ising-HQA) and simulated annealing (RIS-Ising-SA).

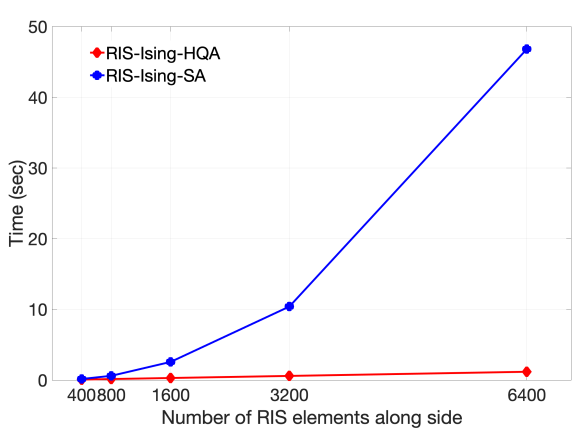


Fig. 11: Time-to-solution required by hybrid quantum annealing (RIS-Ising-HQA) and simulated annealing (RIS-Ising-SA).

B. Numerical Study for Weighted Beamforming

In this subsection, a 5 by 5 RIS array with element size $d=1\lambda$ and normally incident plane wave is used to demonstrate the RIS-Ising annealing optimization for weighted multiple beamforming. We start with the equal-weight beamforming study. The two angular directions of interest are defined as $\theta_1^s=10^o, \phi_1^s=135^o$ and $\theta_2^s=10^o, \phi_2^s=45^o$. The weighting factor W in (9) is set to 1 for equal weightings for both beams. By minimizing the Ising Hamiltonian, we can achieve good beamforming in the specified angular directions with approximately equal beam powers, as depicted in Fig. 12. The ratio of scattering density towards $\phi_1^s=135^o$ is approximately

1.13 times the scattering density towards $\phi_2^s=45^o$. Thus, this shows a minimal energy bias between the two scattered beams. We have also included the results using the brute-force search for comparison. The excellent agreements verify that we have achieved the ground state of our proposed RIS Hamiltonian.

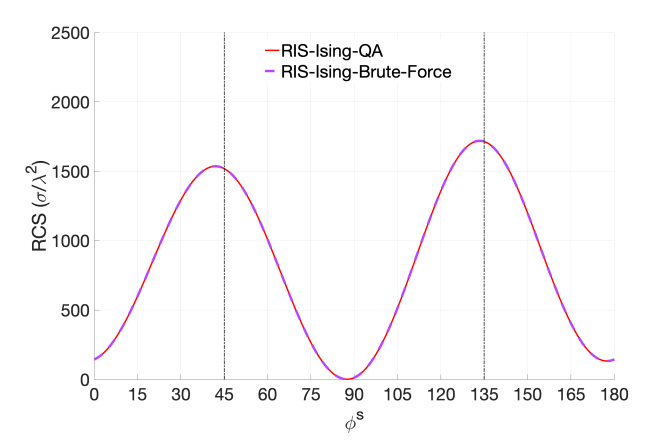


Fig. 12: The RCS plots from a 5 by 5 1-bit RIS array with two beamforming (weighting factor W=1).

We proceed to study the weighted beamforming case by setting the weighting factor W to 1.44. By minimizing the resulting Ising Hamiltonian, we aim to create two beams with a weighted power factor of 2 against the second beam. From Fig. 13, we observe that the scattering density at $\phi_2^s = 135^o$ decreases while the scattering density at $\phi_1^s = 45^o$ increases comparing to the result obtained with W=1 in Fig. 12. Moreover, the ratio of scattering density towards $\phi_1^s = 45^o$ is approximately 1.46 times the scattering density towards $\phi_2^s = 135^o$. The optimized scattering pattern again agrees with the brute-force search result. It is noted that even though we expect the beam power ratio to be 2, the limited performance is due to the physical constraint of the small RIS array.

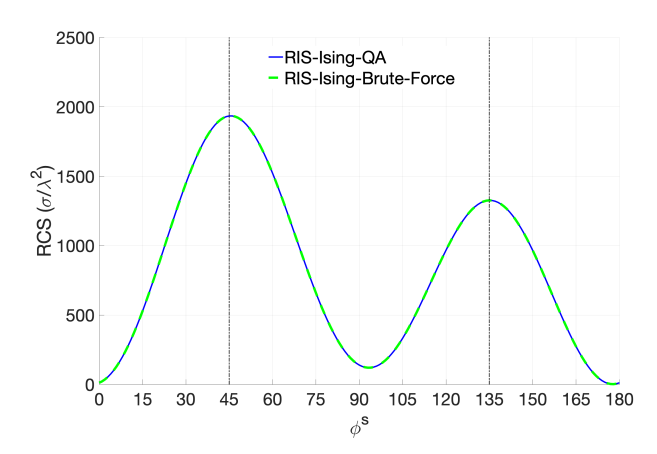


Fig. 13: The RCS plots from a 5 by 5 1-bit RIS array with two beamforming (weighting factor W = 1.44)

Next, we shift our focus to a 5 by 5 RIS panel with 2-bit reflecting elements. The same plane wave excitation and desired scattering angles are used as in the previous problem. Again, we set W to be 1 and 1.44 for the test cases of equal

and weighted multi-beamforming respectively. The optimal 2-bit RIS configuration is derived by the Hamiltonian function in (17). From Fig. 14, we can see that for the case with equal weightings, the ratio of scattering density towards $\phi_1^s=45^o$ is approximately 1.05 times the scattering density towards $\phi_2^s=135^o$. For the weighted beamforming case, the ratio of scattering density towards $\phi_1^s=45^o$ is approximately 2.04 times the scattering density towards $\phi_2^s=135^o$. The result demonstrates the effectiveness of the Ising Hamiltonian model for the 2-bit RIS panel.

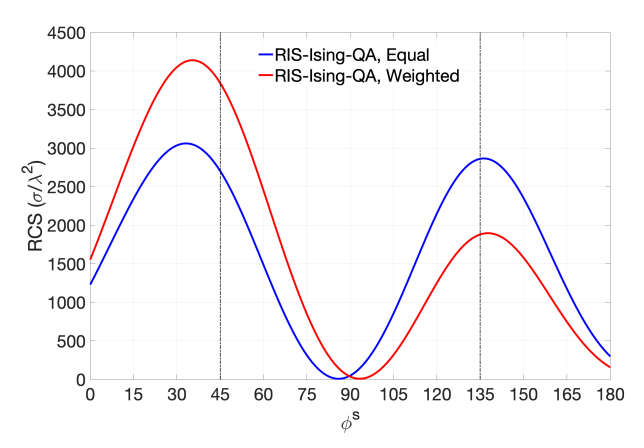


Fig. 14: The RCS plots from a 5 by 5 2-bit RIS array with two beamforming (weighting factor W=1 and W=1.44)

We conclude our numerical study of multi-beamforming with a large-scale RIS panel made up of 50 by 50 1-bit RIS elements. Under a normally incident plane wave, we aim to create two scattered beams with equal power. The optimization is performed by the HQA and SA algorithms. From Fig. 15, we can see both algorithms produced sharp beams towards the desired angles at $\phi_1^s=45^o$ and $\phi_2^s=135^o$ with equal weighting. The SA algorithm takes 7.68 seconds to complete, while the total runtime for the HQA algorithm is 1.24 seconds.

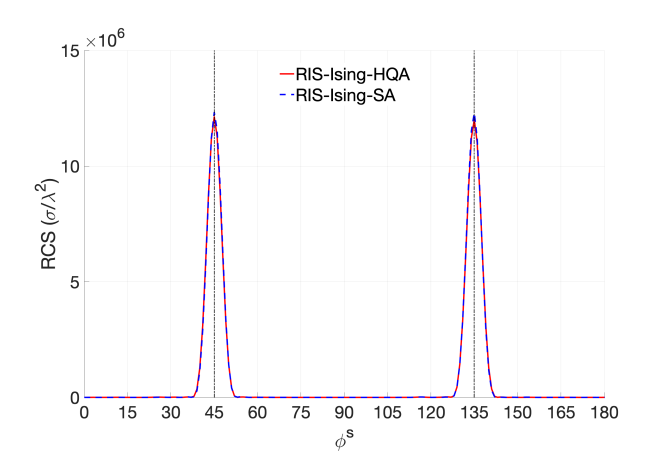


Fig. 15: The RCS plots from a 50 by 50 1-bit RIS array.

C. Numerical Study for Diffusive Scattering

In this subsection, we first demonstrate the performance of the RIS-Ising model for diffuse scattering under a normally incident plane wave. In the numerical experiment, we employ a two-step optimization strategy similar to the one used in related literature [23], [61]. Specifically, instead of optimizing the entire 2D RIS, we have performed two 1D optimizations along each side of the RIS. Following this, the 1D solutions from these sub-problems are used to generate the 2D RIS configuration via an outer product operation. As compared to the related literature, the proposed work accounts for the polarization of the incident field and the element factor of the RIS unit cells through the construction of a diffuse RIS-Ising model. Hence, this would encourage better quality solutions.

To benchmark the performance of the proposed approach, we define a figure of merit (FOM) and a physical limit of diffusive RIS for this numerical study. First, the RCS ratio will be used as the figure of merit [23]. To elaborate, the RCS ratio is the ratio between the highest RCS value from the diffusive RIS to the highest RCS value of a perfect electrical conductor (PEC) plate of the same size. Hence, this FOM describes the performance of the diffusive RIS to suppress high RCS values in all directions. Second, the Isotropic Array Factor (IAF) limit [61] is used as the benchmark performance of diffusive RIS. This limit was derived with the assumption of a constant directivity in the array factor. Thus, it may be considered the physical bound of diffusive RIS performance. By using these two definitions, we can evaluate the quality of the optimized solutions.

The example considered here is a M by M rectangular RIS array with binary phase response in the element reflection coefficient. The size of the RIS element is $d=1\lambda$, and the TE polarized plane wave is normally incident upon the array. As is seen from Fig. 16, the RCS ratio obtained from the diffuse RIS-Ising model follows closely to the IAF limit. The results calculated with the RIS configuration using the GRS-P and GRS-Q coding sequences are also included for comparison. The experiment demonstrates that our proposed approach is effective in optimizing diffusive RIS configurations for the normally incident plane wave.

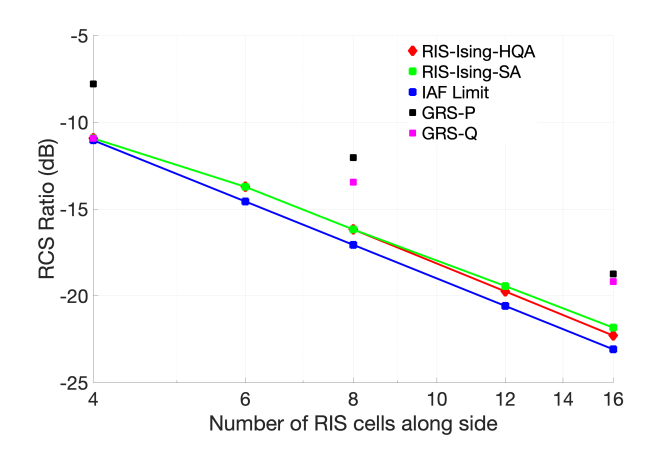


Fig. 16: RCS ratio of diffusive RIS when illuminated at a normal incident angle.

It will also be interesting to apply the optimization approach to the case of an oblique incident angle. We assume that the incident TE polarized plane wave illuminating from

 $\theta^i=75^o, \phi^i=270^o.$ The RCS ratios of the optimized RIS configuration using the diffuse RIS-Ising model are illustrated in Fig. 17. The results using the GRS-P and GRS-Q coding sequences are also included for comparison. The study verifies the flexibility of our Ising Hamiltonian approach in deriving diffusive scattering patterns at oblique incident angles. For both the studies in Figs. 16 and 17, we include the results of the RIS-Ising model with the SA approach. We note that HQA produces slightly better results than SA, particularly for larger-scale problems.

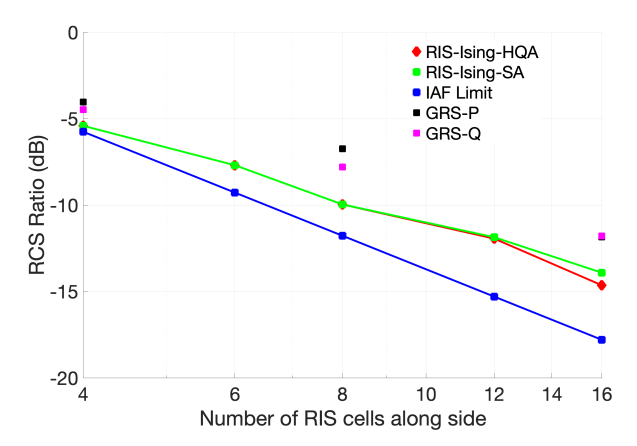


Fig. 17: RCS ratio of the optimized diffusive RIS illuminated at the oblique incident angle ($\theta^s = 75^o$) and ($\phi^s = 270^o$).

Finally, it is noted that the previous study first performs two 1D optimizations of linear RIS arrays, then generates the 2D RIS pattern via the outer product of the optimized 1D patterns. We could also directly optimize the 2D RIS configuration, taking advantage of all available degrees of freedom. The results of direct 2D optimization using RIS-Ising-HQA and RIS-Ising-SA are presented in Fig. 18.

First, we observe that the result of RIS-Ising-HQA with 2D optimization is closer to the IAF limit than the result using the 1D optimization - outer product approach. Secondly, we notice that the RIS-Ising-SA method performs poorly as the RIS panel size grows. It is due to the large number of 4-body interactions involved in the construction of Ising Hamiltonian. For a RIS panel of 6 by 6 elements, a total number of 58,905 4-body terms are obtained in (23). For a RIS panel of 12 by 12 elements, a total number of 17,178,876 4-body terms are presented in the Hamiltonian. Due to the computational complexity, we did not perform the 16 by 16 elements case using HQA. In practice, it is recommended to use the two-level optimization (i.e., block spin) approach proposed in [45].

VII. CONCLUSION

The RIS is emerging as a key technology for the next generation of radio environments and mobile networks. The goal is to transform the wireless environment into a smart, reconfigurable space that actively contributes to communication performance. In order to harness the full potential of the RIS-enabled smart radio environment, we need to rapidly optimize the states of RIS devices with predefined objective functions.

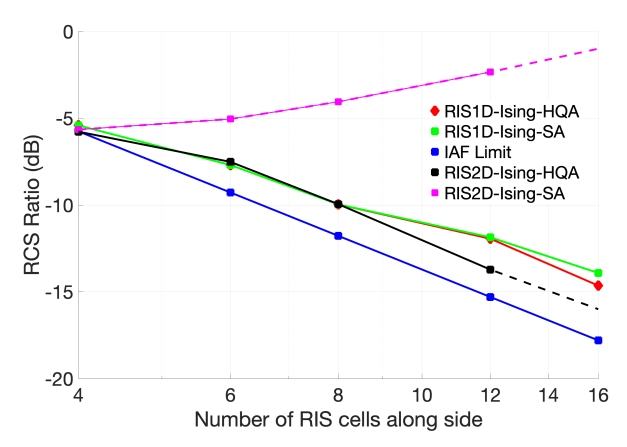


Fig. 18: RCS ratio of the optimized diffusive RIS using 1D optimization - outer product approach and direct 2D optimization approach. The RIS panel is illuminated at the oblique incident angle ($\theta^s = 75^o$) and ($\phi^s = 270^o$).

To overcome the high computational optimization complexity, the proposed work relies on the fusion of statistical mechanics models with quantum computing algorithms. The philosophy is to recast the RIS-aided wireless problem as a physical formulation that can be efficiently addressed with emerging QC hardware. This study sheds light on the relevance of the Ising Hamiltonian for controlling complex EM scattering in real-world communication and defense engineering scenarios. Future research will be devoted to studying the scalability of the optimization approach in solving practical problems involving the deployment of large RIS structures.

REFERENCES

- D. F. Sievenpiper, J. H. Schaffner, H. J. Song, R. Y. Loo, and G. Tangonan, "Two-dimensional beam steering using an electrically tunable impedance surface," *IEEE Transactions on Antennas and Propagation*, vol. 51, no. 10, pp. 2713–2722, 2003.
- [2] C. L. Holloway, M. A. Mohamed, E. F. Kuester, and A. Dienstfrey, "Reflection and transmission properties of a metafilm: with an application to a controllable surface composed of resonant particles," *IEEE Transactions on Electromagnetic Compatibility*, vol. 47, no. 4, pp. 853– 865, 2005.
- [3] F. Bilotti, A. Toscano, and L. Vegni, "Design of spiral and multiple splitring resonators for the realization of miniaturized metamaterial samples," *IEEE Transactions on Antennas and Propagation*, vol. 55, no. 8, pp. 2258–2267, 2007.
- [4] N. Yu, P. Genevet, M. A. Kats, F. Aieta, J.-P. Tetienne, F. Capasso, and Z. Gaburro, "Light propagation with phase discontinuities: Generalized laws of reflection and refraction," *Science*, vol. 334, no. 6054, pp. 333– 337, 2011.
- [5] G. Oliveri, D. H. Werner, and A. Massa, "Reconfigurable electromagnetics through metamaterials-a review," *Proceedings of the IEEE*, vol. 103, no. 7, pp. 1034–1056, 2015.
- [6] A. K. Iyer, A. Alú, and A. Epstein, "Metamaterials and metasurfaces a historical context, recent advances, and future directions," *IEEE Transactions on Antennas and Propagation*, vol. 68, no. 3, pp. 1223–1231, 2020.
- [7] A. Benoni, M. Salucci, G. Oliveri, P. Rocca, B. Li, and A. Massa, "Planning of EM skins for improved quality-of-service in urban areas," *IEEE Transactions on Antennas and Propagation*, vol. 70, no. 10, pp. 8849–8862, 2022.
- [8] M. Di Renzo and S. Tretyakov, "Reconfigurable intelligent surfaces [scanning the issue]," *Proceedings of the IEEE*, vol. 110, no. 9, pp. 1159–1163, 2022.

- [9] E. C. Strinati, G. C. Alexandropoulos, V. Sciancalepore, M. Renzo, H. Wymeersch, D. P. Huy, M. Crozzoli, R. D'Errico, E. Carvalho, P. Popovski, P. Lorenzo, L. Bastianelli, M. Belouar, J. Mascolo, G. Gradoni, S. Phang, G. Lerosey, and B. Denis, "Wireless environment as a service enabled by reconfigurable intelligent surfaces: The RISE-6G perspective," 2021 Joint European Conference on Networks and Communications & 6G Summit (EuCNC/6G Summit), pp. 562–567, 2021.
- [10] C. Pan, H. Ren, K. Wang, J. F. Kolb, M. Elkashlan, M. Chen, M. Di Renzo, Y. Hao, J. Wang, A. L. Swindlehurst, X. You, and L. Hanzo, "Reconfigurable intelligent surfaces for 6g systems: Principles, applications, and research directions," *IEEE Communications Magazine*, vol. 59, no. 6, pp. 14–20, 2021.
- [11] E. Björnson, Ö. Özdogan, and E. G. Larsson, "Reconfigurable intelligent surfaces: Three myths and two critical questions," *IEEE Communica*tions Magazine, vol. 58, pp. 90–96, 2020.
- [12] M. Dunna, C. Zhang, D. F. Sievenpiper, and D. Bharadia, "Scatter-MIMO: enabling virtual MIMO with smart surfaces," Proceedings of the 26th Annual International Conference on Mobile Computing and Networking, 2020.
- [13] Q. Wu and R. Zhang, "Towards smart and reconfigurable environment: Intelligent reflecting surface aided wireless network," *IEEE Communications Magazine*, vol. 58, no. 1, pp. 106–112, 2020.
- [14] K. W. Cho, M. H. Mazaheri, J. Gummeson, O. Salehi-Abari, and K. Jamieson, "mmwall: A reconfigurable metamaterial surface for mmwave networks," *Proceedings of the 22nd International Workshop on Mobile Computing Systems and Applications*, 2021.
- [15] V. Arun and H. Balakrishnan, "RFocus: Beamforming using thousands of passive antennas," in 17th USENIX Symposium on Networked Systems Design and Implementation (NSDI 20). Santa Clara, CA: USENIX Association, Feb. 2020, pp. 1047–1061. [Online]. Available: https://www.usenix.org/conference/nsdi20/presentation/arun
- [16] J. Zhang and D. M. Blough, "Optimizing coverage with intelligent surfaces for indoor mmwave networks," in *IEEE INFOCOM* 2022 -*IEEE Conference on Computer Communications*, 2022, pp. 830–839.
- [17] B. Sihlbom, M. I. Poulakis, and M. Di Renzo, "Reconfigurable intelligent surfaces: Performance assessment through a system-level simulator," 2021. [Online]. Available: https://arxiv.org/abs/2111.10791
- [18] G. Oliveri, P. Rocca, M. Salucci, D. Erricolo, and A. Massa, "Multi-scale single-bit RP-EMS synthesis for advanced propagation manipulation through system-by-design," *IEEE Transactions on Antennas and Propagation*, vol. 70, no. 10, pp. 8809–8824, 2022.
- [19] W. Saad, M. Bennis, and M. Chen, "A vision of 6G wireless systems: Applications, trends, technologies, and open research problems," *IEEE Network*, vol. 34, no. 3, pp. 134–142, 2020.
- [20] M. D. Renzo, M. Debbah, D. T. P. Huy, A. Zappone, M. Alouini, C. Yuen, V. Sciancalepore, G. C. Alexandropoulos, J. Hoydis, H. Gacanin, J. de Rosny, A. Bounceur, G. Lerosey, and M. Fink, "Smart radio environments empowered by AI reconfigurable metasurfaces: An idea whose time has come," EURASIP Journal on Wireless Communications and Networking, vol. 2019:129, 2019. [Online]. Available: http://arxiv.org/abs/1903.08925
- [21] E. C. Strinati, G. C. Alexandropoulos, H. Wymeersch, B. Denis, V. Sciancalepore, R. D'Errico, A. Clemente, D.-T. Phan-Huy, E. De Carvalho, and P. Popovski, "Reconfigurable, intelligent, and sustainable wireless environments for 6G smart connectivity," *IEEE Communica*tions Magazine, vol. 59, no. 10, pp. 99–105, 2021.
- [22] Q. Wu, C. P. Scarborough, D. H. Werner, E. Lier, and X. Wang, "Design synthesis of metasurfaces for broadband hybrid-mode horn antennas with enhanced radiation pattern and polarization characteristics," *IEEE Transactions on Antennas and Propagation*, vol. 60, no. 8, pp. 3594– 3604, 2012.
- [23] T. Cui, M. Qi, X. Wan, J. Zhao, and Q. Cheng, "Coding metamaterials, digital metamaterials and programmable metamaterials," *Light-Science & Applications*, vol. 3, 2014.
- [24] Y. Fan, Y. Xu, M. Qiu, W. Jin, L. Zhang, E. Lam, D. Tsai, and D. Lei, "Phase-controlled metasurface design via optimized genetic algorithm," *Nanophotonics*, vol. 9, pp. 3931 – 3939, 2020.
- [25] G. Minatti, M. Faenzi, E. Martini, F. Caminita, P. De Vita, D. González-Ovejero, M. Sabbadini, and S. Maci, "Modulated metasurface antennas for space: Synthesis, analysis and realizations," *IEEE Transactions on Antennas and Propagation*, vol. 63, no. 4, pp. 1288–1300, 2015.
- [26] T. Brown, Y. Vahabzadeh, C. Caloz, and P. Mojabi, "Electromagnetic inversion with local power conservation for metasurface design," *IEEE Antennas and Wireless Propagation Letters*, vol. 19, no. 8, pp. 1291– 1295, 2020.

- [27] M. Salucci, L. Tenuti, G. Oliveri, and A. Massa, "Efficient prediction of the EM response of reflectarray antenna elements by an advanced statistical learning method," *IEEE Transactions on Antennas and Propagation*, vol. 66, no. 8, pp. 3995–4007, 2018.
- [28] A. Taha, M. Alrabeiah, and A. Alkhateeb, "Enabling large intelligent surfaces with compressive sensing and deep learning," *IEEE Access*, vol. 9, pp. 44304–44321, 2021.
- [29] K. M. Faisal and W. Choi, "Machine learning approaches for reconfigurable intelligent surfaces: A survey," *IEEE Access*, vol. 10, pp. 27343– 27367, 2022.
- [30] G. Zhou, C. Pan, H. Ren, K. Wang, M. Elkashlan, and M. D. Renzo, "Stochastic learning-based robust beamforming design for RIS-aided millimeter-wave systems in the presence of random blockages," *IEEE Transactions on Vehicular Technology*, vol. 70, no. 1, pp. 1057–1061, 2021.
- [31] H. Gacanin and M. Di Renzo, "Wireless 2.0: Toward an intelligent radio environment empowered by reconfigurable meta-surfaces and artificial intelligence," *IEEE Vehicular Technology Magazine*, vol. 15, no. 4, pp. 74–82, 2020.
- [32] J. Hu, H. Zhang, K. Bian, M. D. Renzo, Z. Han, and L. Song, "Metasensing: Intelligent metasurface assisted RF 3D sensing by deep reinforcement learning," *IEEE Journal on Selected Areas in Communi*cations, vol. 39, no. 7, pp. 2182–2197, 2021.
- [33] N. Kaina, M. Dupré, M. Fink, and G. Lerosey, "Hybridized resonances to design tunable binary phase metasurface unit cells," *Opt. Express*, vol. 22, no. 16, pp. 18881–18888, Aug 2014.
- [34] P. del Hougne, F. Lemoult, M. Fink, and G. Lerosey, "Spatiotemporal wave front shaping in a microwave cavity," *Phys. Rev. Lett.*, vol. 117, p. 134302, Sep 2016. [Online]. Available: https://link.aps.org/doi/10. 1103/PhysRevLett.117.134302
- [35] O. Tsilipakos, A. C. Tasolamprou, A. Pitilakis, F. Liu, X. Wang, M. S. Mirmoosa, D. C. Tzarouchis, S. Abadal, H. Taghvaee, C. Liaskos, A. Tsioliaridou, J. Georgiou, A. Cabellos-Aparicio, E. AlarcÃn, S. Ioannidis, A. Pitsillides, I. F. Akyildiz, N. V. Kantartzis, E. N. Economou, C. M. Soukoulis, M. Kafesaki, and S. Tretyakov, "Toward intelligent metasurfaces: The progress from globally tunable metasurfaces to software-defined metasurfaces with an embedded network of controllers," Advanced Optical Materials, vol. 8, no. 17, p. 2000783, 2020.
- [36] J.-B. Gros, P. del Hougne, and G. Lerosey, "Tuning a regular cavity to wave chaos with metasurface-reconfigurable walls," *Phys. Rev. A*, vol. 101, p. 061801, Jun 2020.
- [37] P. Rocca, N. Anselmi, G. Oliveri, A. Polo, and A. Massa, "Antenna array thinning through quantum fourier transform," *IEEE Access*, vol. 9, pp. 124313–124323, 2021.
- [38] C. D. Phillips and V. I. Okhmatovski, "Quantum method of moments for characterization of interconnects," in 2021 IEEE 30th Conference on Electrical Performance of Electronic Packaging and Systems (EPEPS), 2021, pp. 1–3.
- [39] ——, "A quantum computer amenable matrix equation solver with applications to computational electromagnetics," arXiv preprint arXiv:2112.02600, 2021.
- [40] W.-B. Ewe, D. E. Koh, S. T. Goh, H.-S. Chu, and C. E. Png, "Variational quantum-based simulation of waveguide modes," *IEEE Transactions on Microwave Theory and Techniques*, vol. 70, no. 5, pp. 2517–2525, 2022.
- [41] M. Kim, D. Venturelli, and K. Jamieson, "Leveraging quantum annealing for large MIMO processing in centralized radio access networks," Proceedings of the ACM Special Interest Group on Data Communication, Aug 2019.
- [42] M. Kim, S. Kasi, P. A. Lott, D. Venturelli, J. Kaewell, and K. Jamieson, "Heuristic quantum optimization for 6G wireless communications," *IEEE Network*, vol. 35, no. 4, pp. 8–15, 2021.
- [43] T. Q. Duong, L. D. Nguyen, B. Narottama, J. A. Ansere, D. V. Huynh, and H. Shin, "Quantum-inspired real-time optimization for 6G networks: Opportunities, challenges, and the road ahead," *IEEE Open Journal of the Communications Society*, vol. 3, pp. 1347–1359, 2022.
- [44] G. Gradoni, M. Di Renzo, A. Diaz-Rubio, S. Tretyakov, C. Caloz, Z. Peng, A. Alu, G. Lerosey, M. Fink, V. Galdi, T. J. Cui, B. Frazier, S. Anlage, M. Salucci, A. Massa, Q. Cheng, J. Wang, S. Jin, D. Dardari, N. Decarli, O. Yurduseven, M. Matthaiou, M. Kenney, G. Gordon, O. Georgiou, C. L. Nguyen, E. Martini, S. Maci, H. Wakatsuchi, and S. Phang, "Smart Radio Environments," arXiv e-prints, p. arXiv:2111.08676, Nov. 2021.
- [45] C. Ross, G. Gradoni, Q. J. Lim, and Z. Peng, "Engineering reflective metasurfaces with Ising hamiltonian and quantum annealing," *IEEE Transactions on Antennas and Propagation*, vol. 70, no. 4, pp. 2841–2854, 2022.

- [46] S. G. BRUSH, "History of the Lenz-Ising model," Rev. Mod. Phys., vol. 39, pp. 883–893, Oct 1967. [Online]. Available: https://link.aps.org/doi/10.1103/RevModPhys.39.883
- [47] A. Lucas, "Ising formulations of many NP problems," Frontiers in physics, p. 5, 2014.
- [48] E. Björnson, H. Wymeersch, B. Matthiesen, P. Popovski, L. Sanguinetti, and E. de Carvalho, "Reconfigurable intelligent surfaces: A signal processing perspective with wireless applications," *IEEE Signal Processing Magazine*, vol. 39, pp. 135–158, 2022.
- [49] S. Kirkpatrick, C. D. Gelatt, and M. Vecchi, "Optimization by simulated annealing," *Science*, vol. 220, pp. 671 – 680, 1983.
- [50] A. Billionnet and S. Elloumi, "Using a Mixed Integer Quadratic Programming Solver for the Unconstrained Quadratic 0-1 Problem," *Mathematical Programming Computation*, vol. 109, no. 1, pp. 55–68, 2007, note.
- [51] I. Dunning, S. Gupta, and J. Silberholz, "What works best when? a systematic evaluation of heuristics for Max-Cut and QUBO," *INFORMS J. Comput.*, vol. 30, pp. 608–624, 2018.
- [52] P. Hauke, H. G. Katzgraber, W. Lechner, H. Nishimori, and W. D. Oliver, "Perspectives of quantum annealing: methods and implementations," *Reports on Progress in Physics*, vol. 83, no. 5, p. 054401, May 2020.
- [53] R. Biswas, Z. Jiang, K. Kechezhi, S. Knysh, S. Mandrà, B. O'Gorman, A. Perdomo-Ortiz, A. Petukhov, J. Realpe-Gómez, E. Rieffel, D. Venturelli, F. Vasko, and Z. Wang, "A NASA perspective on quantum computing: Opportunities and challenges," *Parallel Comput.*, vol. 64, pp. 81–98, 2017.
- [54] C. C. Chang, A. Gambhir, T. S. Humble, and S. Sota, "Quantum annealing for systems of polynomial equations," *Scientific Reports*, vol. 9, no. 1, Jul 2019.
- [55] J. Cohen, A. Khan, and C. Alexander, "Portfolio optimization of 40 stocks using the dwave quantum annealer," arXiv: General Finance, 2020
- [56] K. Kitai, J. Guo, S. Ju, S. Tanaka, K. Tsuda, J. Shiomi, and R. Tamura, "Designing metamaterials with quantum annealing and factorization machines," *Physical Review Research*, vol. 2, no. 1, pp. 1–10, 2020.
- [57] E. K. Grant and T. S. Humble, "Adiabatic quantum computing and quantum annealing," 07 2020. [Online]. Available: https://oxfordre.com/physics/view/10.1093/acrefore/9780190871994.001.0001/acrefore-9780190871994-e-32
- [58] C. McGeoch and P. Farré, The Advantage System: Performance Update, 2022. [Online]. Available: https://www.dwavesys.com/media/3xvdipcn/ 14-1058a-a_advantage_processor_overview.pdf
- [59] Z. Ding, X. Lei, G. K. Karagiannidis, R. Schober, J. Yuan, and V. K. Bhargava, "A survey on non-orthogonal multiple access for 5G networks: Research challenges and future trends," *IEEE Journal on Selected Areas in Communications*, vol. 35, no. 10, pp. 2181–2195, 2017.
- [60] Y. Cai, Z. Qin, F. Cui, G. Y. Li, and J. A. McCann, "Modulation and multiple access for 5G networks," *IEEE Communications Surveys & Tutorials*, vol. 20, no. 1, pp. 629–646, 2018.
- [61] M. Moccia, S. Liu, R. Y. Wu, G. Castaldi, A. Andreone, T. J. Cui, and V. Galdi, "Coding metasurfaces for diffuse scattering: Scaling laws, bounds, and suboptimal design," *Advanced Optical Materials*, vol. 5, p. 1700455, 2017.
- [62] A. Mandal, A. Roy, S. Upadhyay, and H. Ushijima-Mwesigwa, "Compressed quadratization of higher order binary optimization problems," arXiv:2001.00658 [quant-ph], 2020.
- [63] K. Boothby, P. Bunyk, J. Raymond, and A. Roy, "Next-generation topology of d-wave quantum processors," 2020. [Online]. Available: https://arxiv.org/abs/2003.00133
- [64] J. Cai, B. Macready, and A. Roy, "A practical heuristic for finding graph minors," arXiv:1406.2741v1, 2014.
- [65] A. A. Abbott, C. S. Calude, M. J. Dinneen, and R. Hua, "A hybrid quantum-classical paradigm to mitigate embedding costs in quantum annealing," *International Journal of Quantum Information*, vol. 17, no. 05, p. 1950042, 2019.
- [66] I. Chiscop, J. Nauta, B. Veerman, and F. Phillipson, "A hybrid solution method for the multi-service location set covering problem," pp. 531– 545, 2020.
- [67] P. Shaw, "Using constraint programming and local search methods to solve vehicle routing problems," in *Principles and Practice of Constraint Programming — CP98*, M. Maher and J.-F. Puget, Eds. Berlin, Heidelberg: Springer Berlin Heidelberg, 1998, pp. 417–431.
- [68] D. Pisinger and S. Ropke, Large Neighborhood Search, 09 2010, pp. 399–419.
- [69] J. Raymond, R. Stevanovic, W. Bernoudy, K. Boothby, C. McGeoch, A. J. Berkley, P. Farré, and A. D. King, "Hybrid quantum annealing for

- larger-than-QPU lattice-structured problems," 2022. [Online]. Available: https://arxiv.org/abs/2202.03044
- [70] M. Conforti, G. Cornuéjols, and G. Zambelli, *Integer Programming*, 1st ed. Springer, Cham, 2014.
- [71] D.-W. S. Inc., "D-wave neal," 2022. [Online]. Available: https://docs.ocean.dwavesys.com/projects/neal/en/latest/
- [72] IBM, "Cplex optimizer," https://www.ibm.com/analytics/cplexoptimizer, 2021.



Qi Jian Lim (S'21) received B.E. in Engineering Science from the National University of Singapore in 2015. After graduation, he joined the Defence Science Organization in Singapore as a Member of Technical Staff for 5 years, where he worked on computational electromagnetic modeling for large multi-scale problems and Electromagnetic Metamaterials design. He is currently pursuing a PhD at the University of Illinois Urbana Champaign (UIUC). His research interests include computational electromagnetics for reconfigurable intelligent surface

analysis, design and quantum combinatorial optimization.



Charles Ross (S'21) received his bachelors of science in physics from the California Institute of Technology, California, USA. He is currently pursuing a PhD degree at the University of Illinois Urbana Champaign (UIUC) working with Professor Zhen Peng. His research interests include quantum computation, quantum-assisted optimization, and computational eletromagnetics.



Amitabha (Amitava) Ghosh (F'15) is a Nokia Fellow and works at Nokia Standards and Strategy. He joined Motorola in 1990 after receiving his Ph.D in Electrical Engineering from Southern Methodist University, Dallas. Since joining Motorola he worked on multiple wireless technologies starting from IS-95, cdma-2000, 1xEV-DV/1XTREME, 1xEV-DO, UMTS, HSPA, 802.16e/WiMAX and 3GPP LTE. He has 60 issued patents, has written multiple book chapters and has authored numerous external and internal technical papers. He is cur-

rently working on 5G Evolution and 6G technologies. He is also the chair of the NextGA (an US 6G initiative) National Roadmap Working Group. His research interests are in the area of digital communications, signal processing and wireless communications. He is the recipient of 2016 IEEE Stephen O. Rice and 2017 Neal Shephard prize, member of IEEE Access editorial board and co-author of the books titled "Essentials of LTE and LTE-A" and "5G Enabled Industrial IoT Network".



Frederick W. Vook (SM'04) is a Distinguished Member of the Technical Staff in the Radio Interface group of Nokia Standards in Naperville IL. He currently manages a research and standardization project on MIMO and Beamforming for 3GPP including 5G and 6G. Fred has extensive experience in antenna array technologies, air interface design, algorithm development, propagation modeling, and link- and system-level performance modeling for wireless systems. Prior to joining Nokia in 2011, he was with Motorola for 19 years where he worked

on various topics including MIMO and beamforming solutions for the IEEE 802.16/WiMax and LTE standards, wireless LAN system design, and propagation measurements at 19GHz and 2.4GHz. Fred received his Ph.D. in Electrical Engineering at The Ohio State University in 1992 and has over 90 issued US patents and over 75 conference and journal papers, and 4 book chapters.



Zhen Peng (M'09-SM'18) received the B.S. degree in electrical engineering and information science from the University of Science and Technology of China, Hefei, China, in 2003 and the Ph.D. degree in electromagnetics and microwave engineering from the Chinese Academy of Science, Beijing, China, in 2008. From 2008 to 2013, He was with the ElectroScience Laboratory, The Ohio State University, Columbus, OH, first as a Post-Doctoral Fellow (2008-2009) and then as a Senior Research Associate (2010-2013). From 2013 to 2019, He was an

Assistant Professor at the Department of Electrical and Computer Engineering, The University of New Mexico (UNM), Albuquerque, NM, USA.

He is currently an Associate Professor at the Department of Electrical and Computer Engineering (ECE ILLINOIS), University of Illinois at Urbana-Champaign, Champaign, IL, USA. His research interests are in the area of computational, statistical, and applied electromagnetics. The goal is to simulate classical and quantum electrodynamic physics with intelligent algorithms on state-of-the-art computers, where virtual experiments can be performed for the prediction, discovery, and design of complex systems at unprecedented scales. His research work has had an impact on both civilian and commercial engineering applications, including advanced antennas, radio frequency integrated circuits, electromagnetic interference and compatibility, signal and power integrity, and wireless communication.

Dr. Peng is a recipient of the 2022 16th European Conference on Antennas and Propagation Best Electromagnetics Paper Award, 2021 30th Conference on Electrical Performance of Electronic Packaging and Systems (EPEPS) Best Paper Award, 2019 IEEE Electromagnetic Compatibility (EMC) Symposium Best Paper Award, 2018 National Science Foundation CAREER Award, 2018 Best Transaction Paper Award - IEEE Transactions on Components, Packaging and Manufacturing Technology, 2017 IEEE Albuquerque Section Outstanding Young Engineer Award, 2016 UNM Electrical and Computer Engineering Department's Distinguished Researcher Award, 2015 Applied Computational Electromagnetics Society (ACES) Early Career Award, 2014 IEEE Antenna and Propagation Sergei A. Schelkunoff Transactions Prize Paper Award, a number of Young Scientist Awards and the advisor of Best Student Paper Awards from various conferences.



Gabriele Gradoni (M'11) received the Ph.D. degree in electromagnetics from Universita' Politecnica delle Marche, Ancona, Italy, in 2010. He was a Visiting Researcher with the Time, Quantum, and Electromagnetics Team, National Physical Laboratory, Teddington, U.K., in 2008. From 2010 to 2013, he was a Research Associate with the Institute for Research in Electronics and Applied Physics, University of Maryland, College Park, MD, USA. From 2013 to 2016, he was a Research Fellow with the School of Mathematical Sciences, University

of Nottingham, U.K., where he was a Full Professor of mathematics and electrical engineering. Since May 2023 he has been Full Professor and Chair of Wireless Communications at the 6G Innovation Centre, Institute for Communication Systems, University of Surrey, Guildford, U.K. Since June 2020, he has been an Adjunct Associate Professor with the Department of Electrical and Computer Engineering, University of Illinois at Urbana-Champaign, USA. Since 2020, he has been a Royal Society Industry Fellow at British Telecom, U.K. Since December 2022, he has been a Visiting Fellow with the Department of Computer Science and Technology, University of Cambridge, U.K. His research interests include probabilistic and asymptotic methods for propagation in complex wave systems, metasurface modelling, quantum/wave chaos, and quantum computational electromagnetics, with applications to electromagnetic compatibility and modern wireless communication systems. He is a member of the IEEE and the Italian Electromagnetics Society. He received the URSI Commission B. Young Scientist Award in 2010 and 2016, the Italian Electromagnetics Society Gaetano Latmiral Prize in 2015, and the Honorable Mention IEEE TEMC Richard B. Schulz Transactions Prize Paper Award in 2020. From 2014 to 2021, he was the URSI Commission E. Early Career Representative.